# Continuous Chirality Measure in Reaction Pathways of Ruthenium-Catalyzed Transfer Hydrogenation of Ketones

Jan-Willem Handgraaf,[a,b] Joost N. H. Reek,[a,*] Luca Bellarosa,[b] Francesco Zerbetto[b,*]

[a] van 't Hoff Institute for Molecular Sciences, University of Amsterdam, Nieuwe Achtergracht 166, 1018 WV, Amsterdam, The Netherlands
Fax: (+31)-20-525-6456, e-mail: reek@science.uva.nl
[b] Dipartimento di Chimica "G. Ciamician", Università di Bologna, Via. F. Selmi 2, 40126 Bologna, Italy
Fax: (+39)-51-209-9456, e-mail: francesco.zerbetto@unibo.it

Received: November 9, 2004; Accepted: March 8, 2005

Supporting Information for this article is available on the WWW under http://asc.wiley-vch.de/home/.

**Abstract:** Here we report theoretical studies on the ruthenium-catalyzed reduction of acetophenone (and 2-hexanone) with the intent of understanding the relative roles of catalyst and substrate along the reaction path. Overall ten reaction pathways are examined. The first eight are for acetophenone: they arise from the presence of two catalysts, with the more enantioselective one labeled **1**, and the poorer one labeled **2**, multiplied by the two configurations that the metal center of the catalysts can assume, multiplied by the two approaches, *Re*- and *Si*-side, of the substrate to the catalyst. Two pathways are examined for 2-hexanone and entail the two approaches to the ketone of the more effective catalyst. Density functional theory calculations provide structures of the minima and transition states, which subsequently have been assessed with the "continuous chirality measure" model developed by Avnir and collaborators. The picture that emerges is that the asymmetric induction is due to the interplay between the organometallic system and the organic substrate. This is effective only for catalyst **1**, which can interact effectively with acetophenone along only one in four of the reaction pathways, but not for **2** for which two out of four pathways are opened. For the hydrogenation of 2-hexanone, the same catalyst **1** cannot produce enantiomeric excesses because the conformation of the substrate in the transition state induced by the catalyst has a relative low chirality.

**Keywords:** asymmetric catalysis; continuous chirality measure; density functional theory; hydrogen transfer; ruthenium

## Introduction

The design of asymmetric transition-metal catalysts remains challenging because of the high sensitivity of the yields of the target products to small energy changes along the reaction pathways.[1] While several studies on the origin of the enantioselectivity have indeed provided insight into various types of reactions,[2] the ability to predict *a priori* the performance of catalysts has still not been reached. Catalysts are often found serendipitously and high selectivities in asymmetric conversions are obtained only after intensive ligand optimization based both on trial and error and on sophisticated guesses. Recently, Lipkowitz et al. found an interesting relation between the chirality content of Lewis acid catalysts, calculated on the basis of Avnir's "continuous chirality measure", CCM,[3] and their stereoinduction in the asymmetric Diels–Alder reaction.[4] In subsequent work, the CCM model was used to evaluate the chirality content of Katsuki–Jacobsen catalysts.[5] Recently, we showed that this methodology could also be used in an "electronic" variation for a set of asymmetric aminohydroxylation reactions where the "regular" geometrical CCM was less successful.[6]

We have chosen to study the ruthenium (Ru)-catalyzed asymmetric transfer hydrogenation reaction[7] because it represents an important class of reactions that gives selective reduction to chiral alcohols under mild conditions. Its mechanism has been studied in detail both experimentally[8] and theoretically.[9] It is now established that when ruthenium complexes, based on amino alcohol or *N*-sulfonylated ethylenediamine ligands, are used the reaction proceeds *via* metal-ligand bifunctional catalysis, where a proton of the amine group of the ligand and the metal-coordinated hydride are transferred in a concerted manner to the pro-chiral

  DOI: 10.1002/adsc.200404342 

ketone.[10] The knowledge of the reaction mechanism and the details of the associated reaction pathways make the ruthenium-catalyzed transfer hydrogenation a good case for an investigation with the CCM method. We report therefore how chirality is transmitted/originated by two chiral transition metal catalysts (only one of them effectively producing enantiomeric excess, ee) to a pro-chiral substrate along the potential energy surface. We compare the transfer hydrogenation of acetophenone, in general able to give high enantioselectivity with the experimentally difficult case of 2-hexanone, for which it proves difficult to obtain even a modest enantiomeric excess. Interestingly, the CCM calculation shines light on the origin of the difference between the two substrates.

## Computational Methods

We performed density functional theory (DFT)-based electronic structure calculations using the BLYP functional that combines a gradient correction term for the exchange energy proposed by Becke[11] with a correction for the correlation energy due to Lee, Yang and Parr.[12] In a recent contribution,[9d] we used this functional in a computational study of a similar system and found that differences between this functional and the B3LYP functional, generally regarded as a rather accurate functional, were of the order of a few kcal/mol, and therefore within the accuracy of DFT.

The pseudopotential method was used to restrict the number of electronic states to those of the valence electrons. The interaction with the core electrons was taken into account using semi-local norm-conserving Martins–Troullier pseudopotentials.[13] The pseudopotential cut-off radii for H, C, N and O were 0.50, 1.23, 1.12 and 1.10 a.u., both for the $l=s$ and $l=p$ terms, respectively. The Ru pseudopotential was of the semicore type including the highest *s*- and *p*-shell electrons as valence electrons. It was generated using an ionized configuration ($Ru^+$) with the electrons treated relativistic within the scalar approximation. In case of Ru the radii of the $l=s$, $l=p$, and $l=d$ pseudopotentials were 1.10, 1.20, and 1.24 a.u. The electronic states were expanded in a plane-wave basis with a cutoff of 70 Ry. All calculations were performed with the CPMD package.[14] We have already validated the numerical accuracy of this plane-wave-based package against the state-of-the-art atomic orbital-based ADF package,[15] and showed that both for the structure and the energetics good to excellent agreement is obtained.[9d]

Geometry optimizations were performed in a periodic box with simple cubic symmetry and a side of 14.0 Å. Test calculations showed that with this set-up structural properties are converged within 0.005 Å and 0.01 Å for the intra- and intermolecular bonds, respectively. Energies were converged within 0.3 kcal/mol and do not include zero-point energy (ZPE) corrections. Noyori and co-workers showed for a similar system at B3LYP/6–31G(d, p)-level that these corrections lowered the activation energy of the transfer hydrogenation of formaldehyde by 0.9 kcal/mol.[9b] For our calculations we expect a comparable decrease in the activation energies if ZPE corrections are included. Since the different reaction paths for the *Si*- and *Re*-approaches are comparable, we expect this decrease to be similar for both approaches.

In analogy to Avnir and co-workers[3] and previous work,[16] the continuous chirality measure (CCM) of a typical molecule was calculated as

$$S = \frac{100}{nD^2}\sum_{i=1}^{n}\left(p_i - \hat{p}_i\right)^2 \quad (1)$$

where $n$ is the number of atoms in the molecule, $D$ is a normalization factor that makes CCM size-invariant,[3] $p_i$ are the atomic coordinates, and $\hat{p}_i$ are the coordinates of the mirror image of the molecule. Notice that in the original model, $\hat{p}_i$ are the coordinates of the closest non-chiral set of points that can be obtained starting from $p_i$. The technical change in Eq. (1) expedites calculations in our computer programs because it by-passes the need to assign the atoms of the non-chiral structure. In fact, in order to achieve non-chirality, one needs to introduce in the molecular structure a symmetry element: a plane, an inversion center, or a roto-reflection axis. Usually, the minimal value of CCM is obtained by modification of the coordinates of the molecule to entail a symmetry plane. The atoms must then be assigned either to lie in the plane, or be coupled in pairs with respect to it. The location of the plane cannot be determined *a priori* or by inspection but must be optimized numerically. In the present approach, instead, we focus on the true nature of an enantiomeric pair and consider the two mirror images. The procedure tries to find the minimal Euclidean distance between the two enantiomers by rotating and translating one of them. The numerical time-consuming optimization therefore persists since one of the two the mirror images must be displaced in space until the value of CCM is minimal. In practice, this is equivalent to a change of the location of the mirror.

Importantly, in this approach, if the atoms are numbered progressively, their numbering may not be conserved in the mirror image so that switches between the reference and the mirror structure may occur. In order to minimize the value of S, we used a Monte Carlo technique where the position of each enantiomer was randomly rotated in space until the minimum value was attained.

## Results and Discussion

We investigated two prototypical systems that, despite their similarity, show very different enantioselectivity for the hydrogenation of acetophenone. Reduction of 2-hexanone will be considered later on. Catalyst **1**, see Scheme 1, gives a 52% excess of the reduced alcohol of configuration *S*, whereas catalyst **2** gives only a 6% excess of the *S*-product.[9c] The structural difference between the two catalysts is the chiral center adjacent either to the oxygen in **1** or the nitrogen in **2**.

In solution, the *R*-configuration of the metal atom is in rapid equilibrium with the *S*-configuration. Both enantiomers of the catalyst therefore were considered. To simplify the notation and avoid awkwardness, the *R*-

  

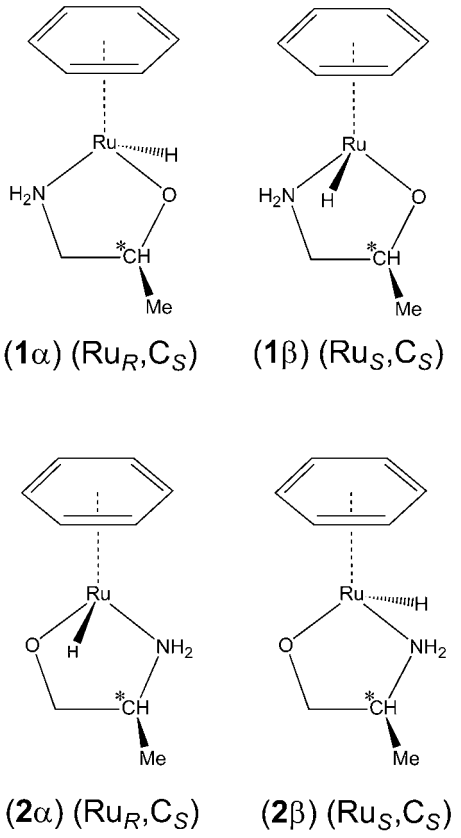


**Scheme 1.**

configuration at Ru is labeled **α**, and the *S*-configuration **β**.

DFT calculations were carried out at six points along the reaction pathways:

– isolated molecules of the reactants, hydrogenated catalyst and pro-chiral ketone;
– encounter-complex of catalyst and substrate, labeled (**0**);
– reacting intermediate complex of catalyst and substrate, labeled (**a**);
– reaction transition state, labeled (**b**);
– complex of reacted catalyst and product, labeled (**c**);
– isolated molecules of the products, dehydrogenated catalyst and chiral secondary alcohol.

The labeling is used throughout this work and emphasizes the different role of the stationary points in the reaction pathways. The isolated systems correspond to infinite separation, the encounter complexes are minima but must rearrange to reach complex (**a**) to carry out the reaction. Points (**a**), (**b**) and (**c**) are the critical points of the reaction.

For both catalysts **1** and **2**, we compared the substrate approach from the *Re*- and *Si*-sides that leads to the (major) *S*-alcohol product and the (minor) *R*-alcohol, see Figures 1 and 2. As a further simplification of the text, we introduce in brackets the enantiomer that results from the approach. For instance, **1α**-*Re(S)* is catalyst **1** in the *R*-configuration, approaching from the *Re* side to give the *S*-enantiomer of the product. In total, eight reaction pathways for the reduction of acetophenone have been calculated, see Figure 3 for the energetics: two catalysts, **1** and **2**, multiplied by the two configurations at the metal center, **α** and **β**, multiplied by the two, *Re*- and *Si*-side, approaches.

The results of the DFT calculations are in good agreement with previous calculations and with experimental results. For catalyst **1**, the most stable encounter-complex is **1α**-*Si(R)*. This adduct is in equilibrium with the same **1α** catalyst approaching to the substrate from the *Re*-side, and with the two encounter-complexes formed by **1β**. The lowest transition state, which governs the enantiomeric excess, is found to be **1α**-*Re(S)*. This is 1.3 kcal/mol lower than its closest counterpart, **1α**-*Si(R)*. Both transition states for **1β** are substantially higher in energy and their pathways do not come into play because the barrier is ~5 kcal/mol higher than for **1α**. The higher barriers in the **1β** reaction pathways are mainly due to steric hindrance between the methyl group of the ligand backbone and the phenyl group of the substrate. It is this interaction that by-and-large tunes the energy location of the transition states (see comment below). The accuracy of the DFT calculations rules out this path as thermally accessible, but may leave uncertain the details of the competition between the other two pathways. The path of **1β** will therefore no longer be discussed in the following unless otherwise stated. Taking the two **1α** barriers at face value, at room temperature, 1.3 kcal/mol of energy difference gives a reaction rate ratio of ~1:10, which fully accounts for the 52% enantiomeric excess of the *S*-enantiomer (although we realize that this energy difference is close to the accuracy of the method).

For catalyst **2**, the thermodynamically stable encounter-complex is **2α**-*Si(R)*, similar to catalyst **1**. The same considerations discussed for the equilibria of **1** apply for this catalyst. Analogously, the lowest transition is for **2α**-*Re(S)*. Its transition state, however, is only 0.5 kcal/mol lower than both of the **2β** transition states and 1.2 kcal/mol lower than **2α**-*Si(R)*. Contrary to **1β**, for **2β** there is no steric hindrance between the methyl group of the ligand backbone and the phenyl group of the substrate. The presence of four transition states within 1.2 kcal/mol (and three of them within 0.5 kcal/mol) qualitatively accounts for the poor enantioselectivity of this catalyst.

The optimized geometries of the different steps along the reaction pathways were used as input for the calculation of the CCM, S, of the catalysts and substrates.[3–6,16] Here we use a slight modification of the original CCM proposed by Avnir and co-workers, see previous section. An analysis in terms of CCM rather than in

  

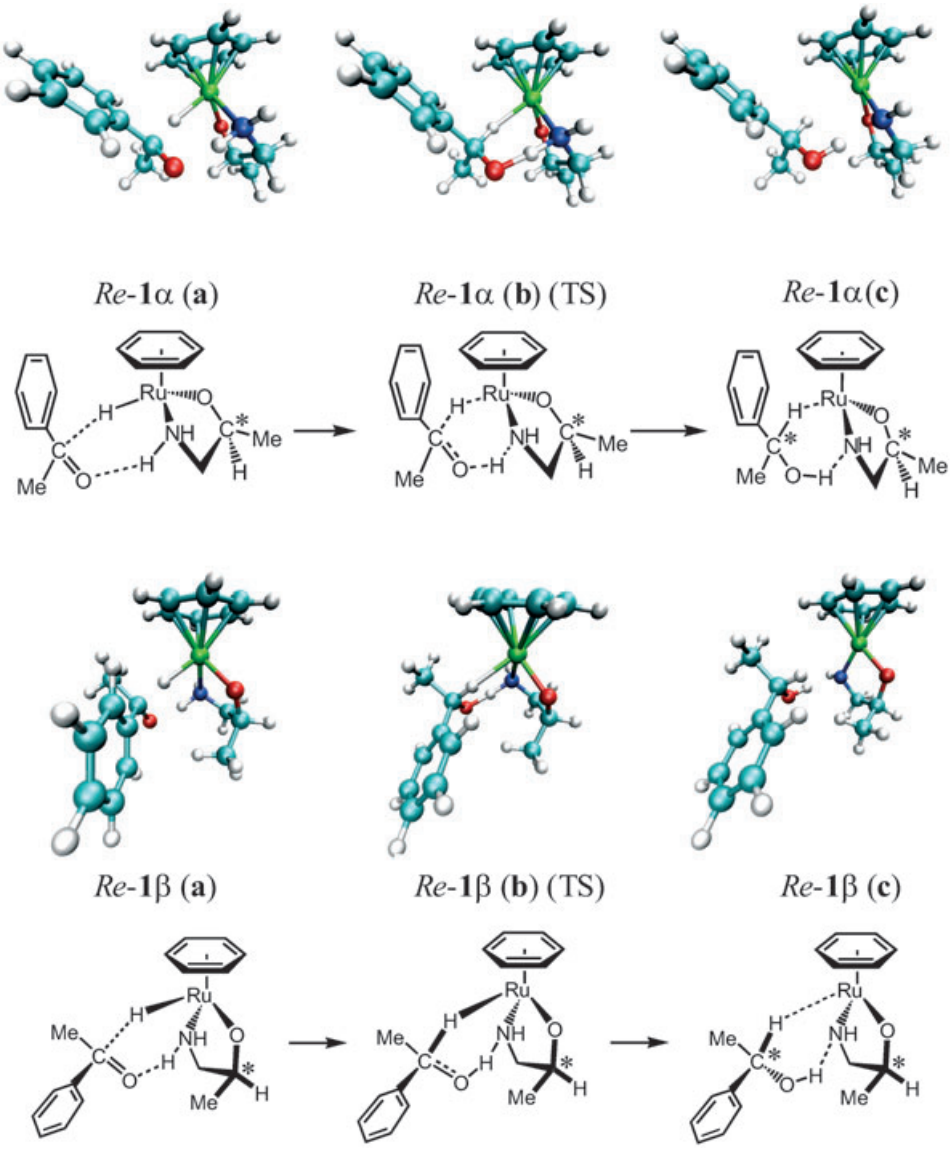


**Figure 1a.** Optimized and schematic structures of the different complexes of the *Re*-approach of acetophenone to catalyst **1α** (top) and **1β** (bottom) along the reaction pathway: intermediate complex of catalyst and substrate in step (**a**), the transition state with the concerted transfer of the proton and the hydride in step (**b**), and the complex of dehydrogenated catalyst and chiral product in step (**c**). The encounter-complex, (**0**), is not shown, but is available upon request to the authors.

terms of the geometry is deemed more effective in the assessment of the origin of enantioselectivity. This follows a growing number of reactions where the judicious use of CCM rationalizes the enantioselective discrimination. The rationale for the use of CCM is that it enucleates from the structures the contributions that provide chirality, whose differential production is the ultimate purpose of enantioselective synthesis. Thus in view of the experimental and the DFT results, the question is whether a further rationalization can be obtained by CCM.

Figure 4 shows the CCM trend for catalysts **1α**, **2α** and **2β**. (The results for **1β** are not shown because its reaction paths are thermally non-accessible on the basis of the DFT calculations).

At this level, the trends for the catalysts are not greatly revealing. The curve for the more effective catalyst **1α** is located between those for the less effective **2α** and **2β**. Moreover, there is hardly any difference between the pathways that lead to the mirror image products.

In Figure 5 are shown the CCM trends observed for the substrate. Inspection of these plots revealed several interesting points. The enantiomer that is favored by **1α** shows a higher chirality than the opposite analogue. This suggests that the enantiomer produced in larger quantity can be assigned in consideration of the total induced

  

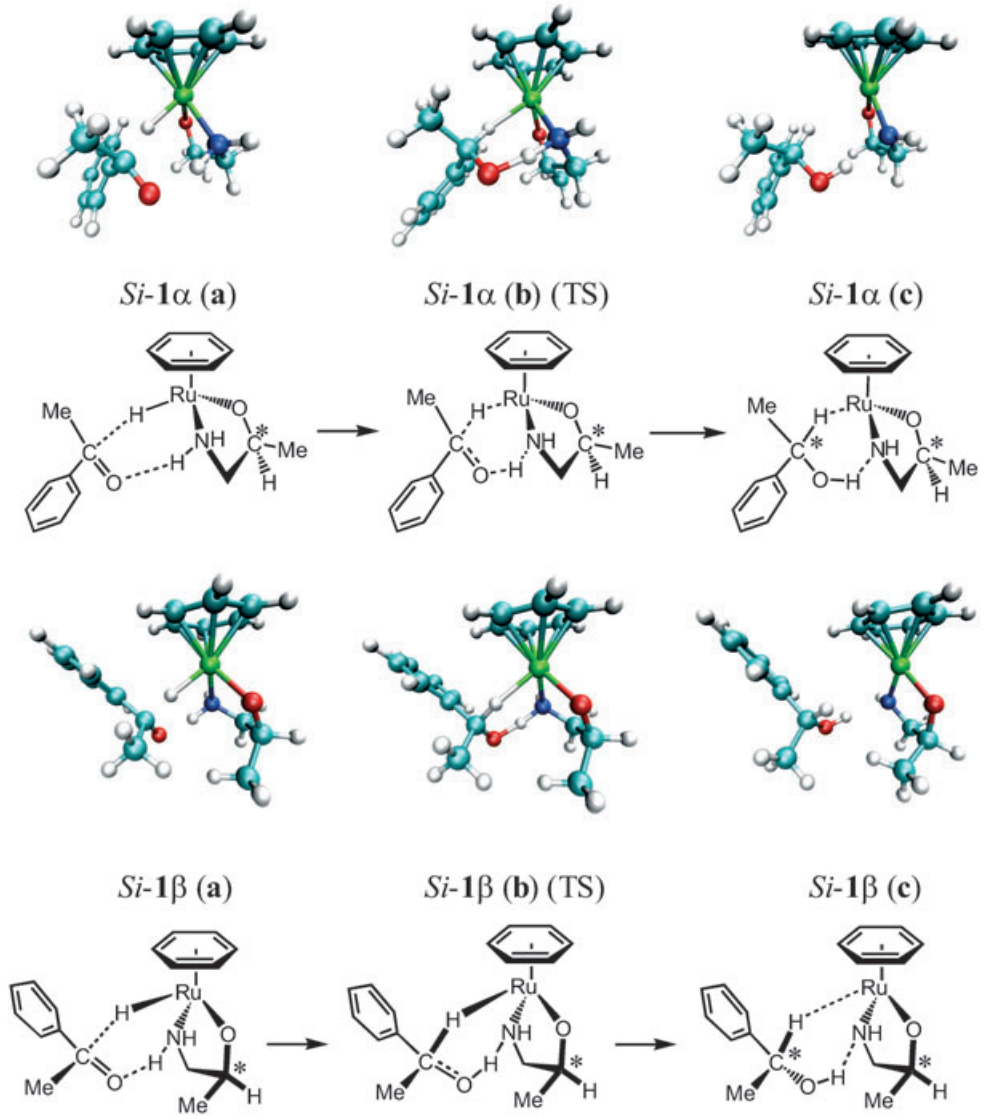


**Figure 1b.** Optimized and schematic structures of the different complexes of the *Si*-approach of acetophenone to catalyst **1α** (top) and **1β** (bottom) along the reaction pathway: intermediate complex of catalyst and substrate in step (**a**), the transition state with the concerted transfer of the proton and the hydride in step (**b**), and the complex of dehydrogenated catalyst and chiral product in step (**c**). The encounter-complex, (**0**), is not shown, but is available upon request to the authors.

chiralization along the reaction path: **1α** favors the *S*-product, as observed experimentally for **1** (the corresponding **1β** path is thermally not accessible). We observed a similar behavior for **2α**, while **2β** favors the *R*-product. Since catalysts **2α** and **2β** co-exist, no ee is observed when using **2**. The difference observed for **2α** and **2β** additionally indicates that the chirality induced by the catalyst is determined by the chirality at the metal center. Obviously, the chirality of the ligand determines the chirality at the metal center.

The overall chirality measure of the complexes was also investigated, but no trends emerged. However, following the work of Alvarez et al.[17] we considered the CCM of the molecular subunits in the complexes that are most relevant to the reaction. We decided to include atoms close to the reactive part of the complex, which in practice resulted in the removal of the cymene unit and most of the phenyl group of the substrate (one carbon atom was retained to maintain chirality). Figure 6 shows that the new results concur with those reported in Figure 5. Catalyst **2α** is the most discriminating, with the larger difference of CCM in favor of the *S*-product; **1α** also shows a difference although not as strong as that reported in Figure 5, while there is no difference of CCM at the transition state for **2β**, with the products that would favor the minor enantiomer.

A similar set of CCM calculations limited to the catalyst, from which the coordinating cymene group was removed showed no discriminating power, in analogy to what was reported in Figure 4. Comparison of the results

  

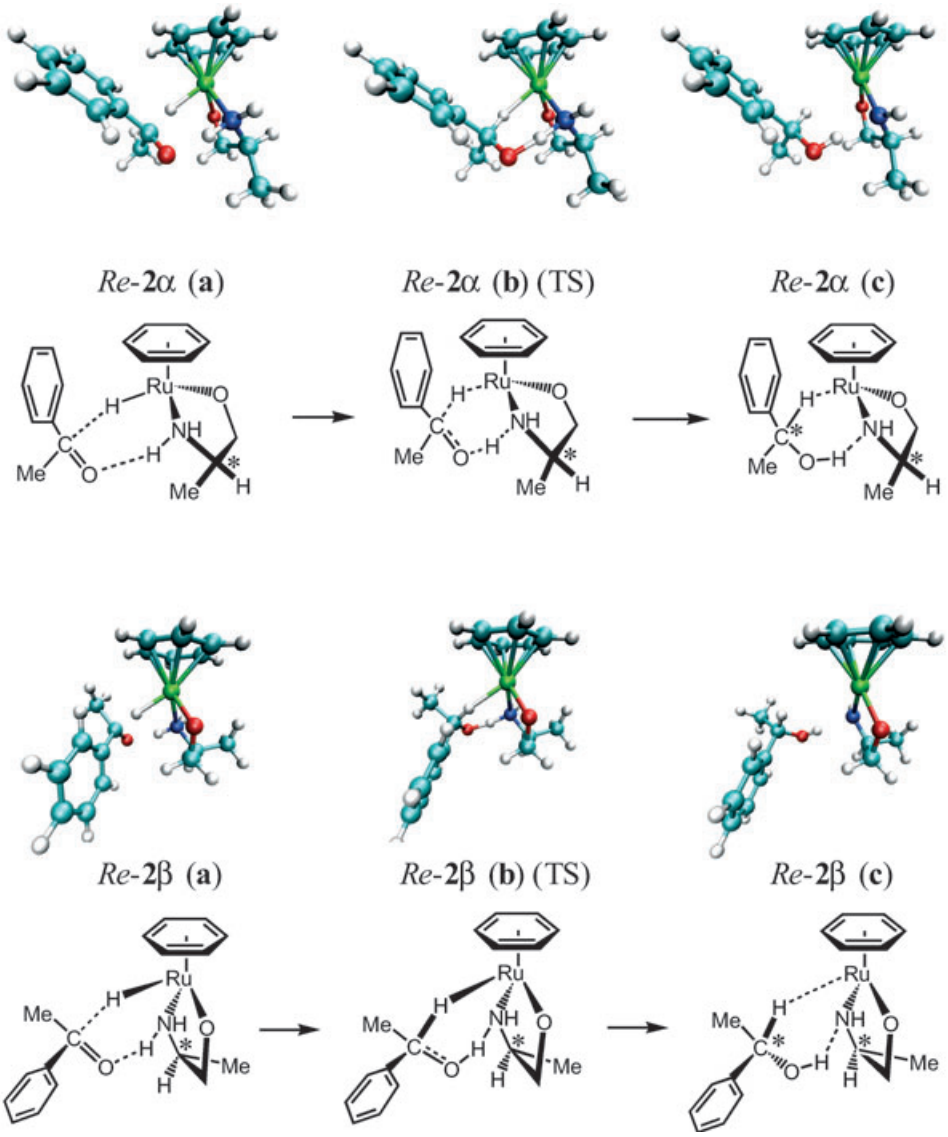


**Figure 2a.** Optimized and schematic structures of the different complexes of the *Re*-approach of acetophenone to catalyst **2α** (top) and **2β** (bottom) along the reaction pathway: For other details, see caption of Figure 1.

of Figures 5 and 6 therefore confirm the role of the substrate but also finds the influence of the core part of the catalyst. The two approaches provide alternative but coherent ways of describing the role of "continuous chirality measure" in this class of reactions.

An interesting observation is that the chirality of the substrate is the highest around the transition state. In turn, this indicates that the reaction pathway in principle is well suited for enantioselective catalysis. The underlying reason for this becomes clear when analyzing the chirality of the substrate as function of its conformation.

In Figure 7 are given plots of the internal acetophenone $HC_{chiral}C_{phenyl}C_{phenyl}$ dihedral angle, here denoted as Φ, versus the CCM values of the critical points (**a**), (**b**) and (**c**) for the **α** and **β** catalysts. Notice that the torsional angle of the phenyl group governs the amount of chirality in the substrate and the inversion of the angle changes the enantiomer. The **α** catalysts show a quasi-linear correlation, $r = 0.93$, between the angle Φ and CCM, while the **β** catalysts, which according to the CCM analysis generate the minor enantiomer, have several points off the main line. If the points of Figures 7a and 7b are overlapped, no trend emerges. The catalysts therefore lock the angle responsible for the amount of chirality in the organic substrate at different values that are independent from each other and the better catalyst, **1**, shows a linear trend between CCM and this angle.

The combination of DFT calculations and CCM therefore concurs with the experiments that only **1** can yield good enantiomeric excesses. In particular, the two models suggest that the $R \leftrightarrow S$ equilibrium at the metal chiral center is detrimental for the formation of an enantiomeric excess since the two chiral configura-

  

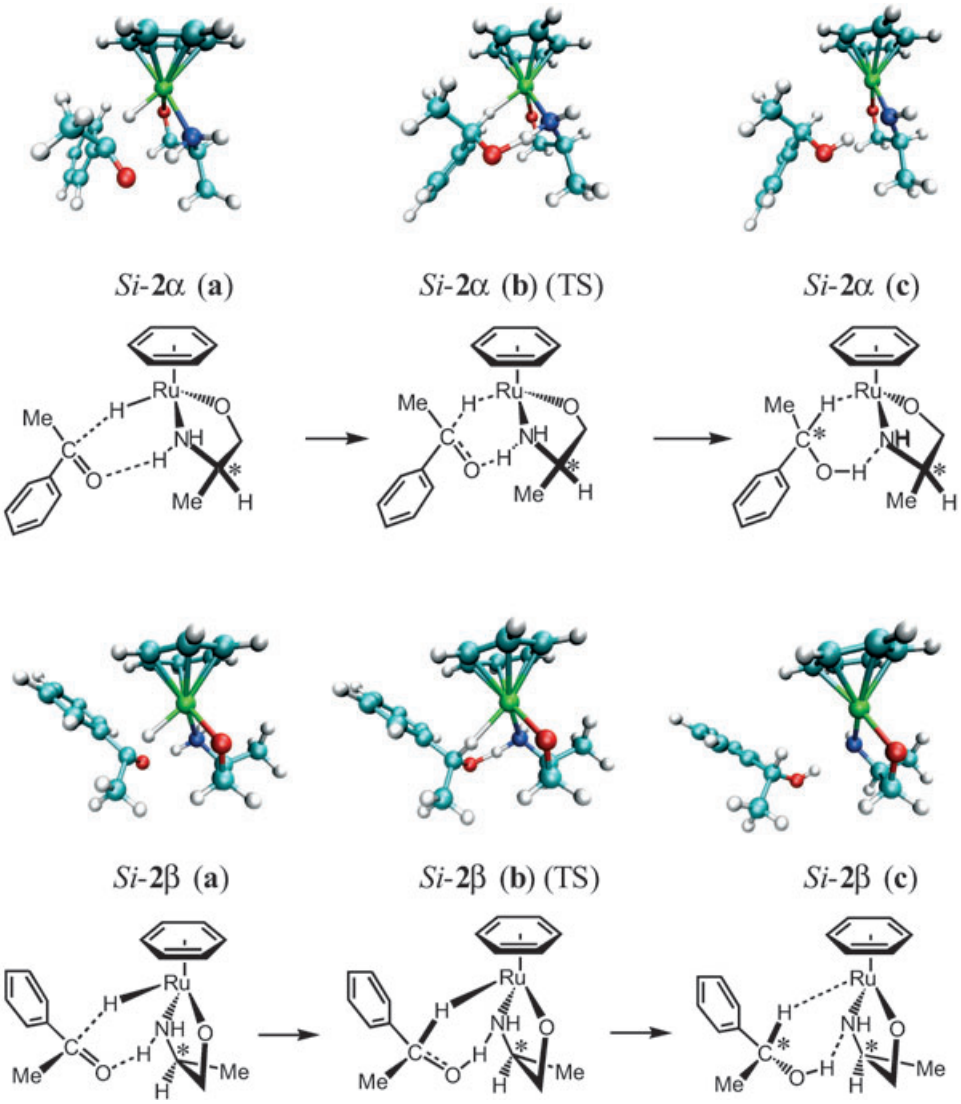


**Figure 2b.** Optimized and schematic structures of the different complexes of the *Si*-approach of acetophenone to catalyst **2α** (top) and **2β** (bottom) along the reaction pathway: For other details, see caption of Figure 1.

tions at the metal center catalyze the formation of a different enantiomer. CCM also implies that, for this reaction, the catalysts do not really discriminate between the two paths. However, through the interaction with the substrate, they are able to impart a different CCM to the chiralizing molecule.

DFT calculations were also performed for the Ru-catalyzed reduction of 2-hexanone along the two reaction paths, *Re*- and *Si*-side approaches, of catalyst **1α**. For this substrate, catalyst **1** does not yield appreciable enantiomeric excess.[18] We found that the energy barrier for the *Re*- and *Si*-approaches are 15.4 and 14.3 kcal/mol with a preference for the formation of the *R*-enantiomer. Alone, DFT calculations do not explain the experimental result, simply because 1 kcal/mol is within the intrinsic accuracy of the model. CCM, on the contrary, see Figure 8, shows that the catalyst is unable to chiralize differently 2-hexanone along the two reaction paths and provides a simple explanation for the lack of enantiomeric induction.

In order to obtain detailed insight in the origin of the difference between the two substrates, additional DFT calculations were then performed on *S*-1-phenylethanol and *S*-2-hexanol with constrained values of the dihedral angle discussed in Figure 7, while all other degrees of freedom were allowed to vary. Figure 9 shows the corresponding energy profiles and changes in CCM. Energy and CCM minima and maxima do not necessarily coincide. The CCM profile is broader for the ketone that gives lower chiral induction. The red vertical lines show the actual dihedral angle of the substrates in the transition state of **1α**-*Re(S)*. Interestingly, catalyst **1** in-

  

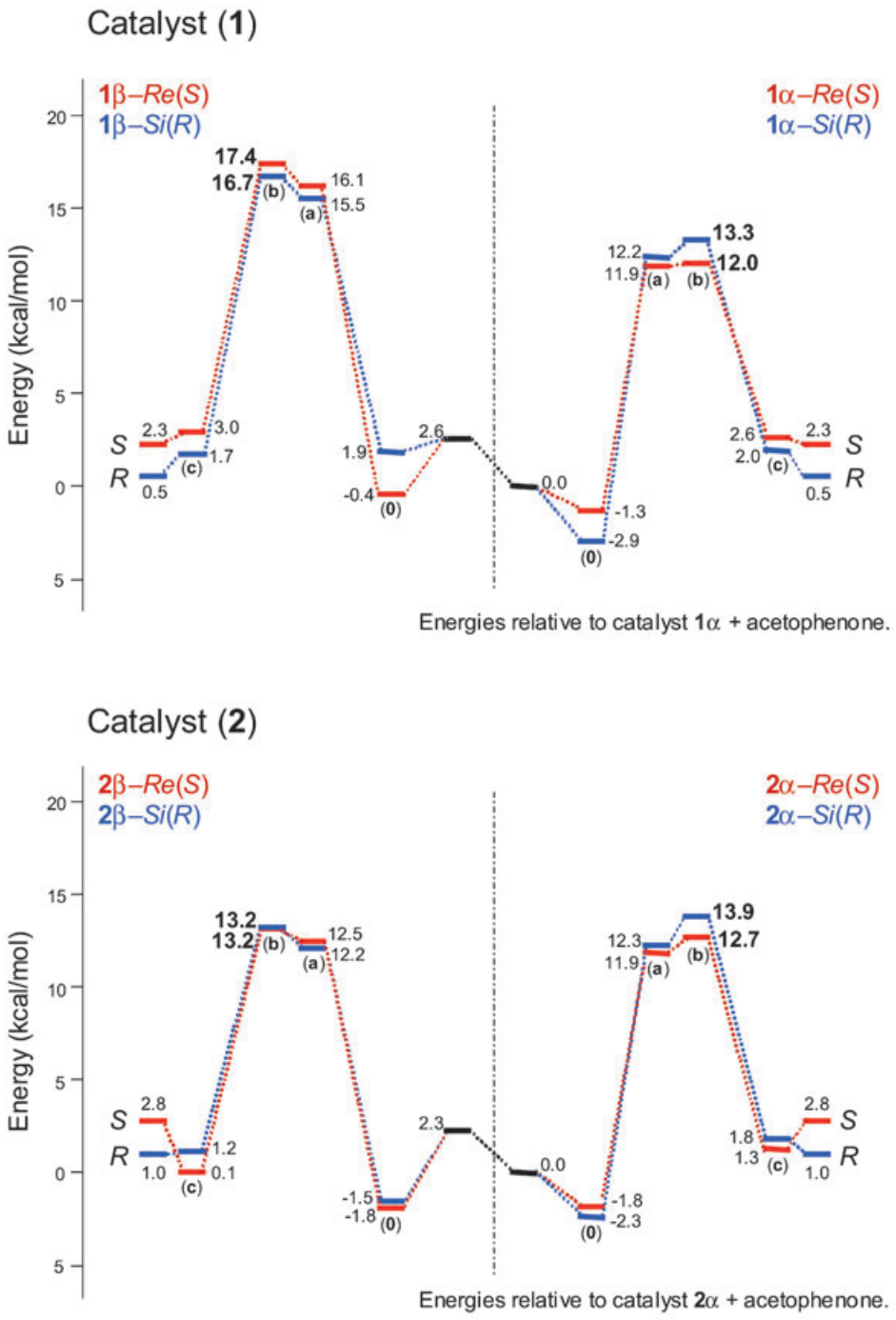


**Figure 3.** Energy profiles of the *Re*- and *Si*-approaches of acetophenone for catalysts **1** and **2**. Energies are without zero-point energy corrections and entropy contributions. Values in bold are for the transition states. Black horizontal bars are for the catalyst and substrate at infinite distance, i.e., isolated systems.

duces a conformation in the aromatic substrate that is 2 kcal/mol higher in energy and has a higher chirality facilitating enantio-induction during catalysis. In contrast, the same catalyst does not induce such a conformation for the aliphatic substrate, providing a good explanation for the differences observed. In addition, new directions for the design of a good catalyst for this substrate might be extracted from this picture. According to the analysis suggested by Figure 9, a catalyst able to induce selectivity in the transfer hydrogenation of 2-hexanone should induce a conformation with a dihedral angle around 0°. This would maximize the chirality in the transition

  

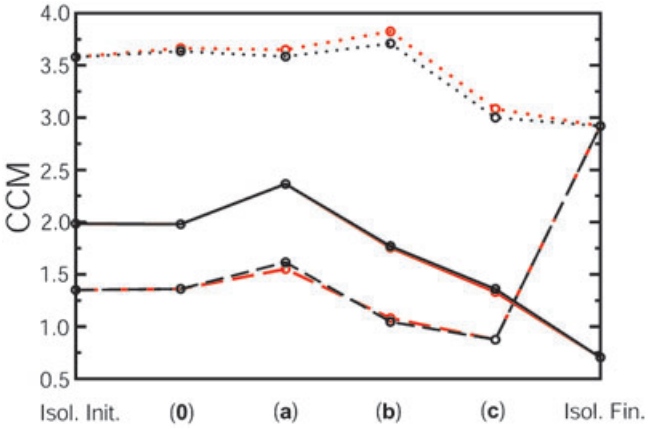


**Figure 4.** Catalysts CCM along the reaction pathway of acetophenone reduction. In black the path that gives the *S*-enantiomer; in red, the path that gives the *R*-enantiomer: solid line for **1α**; dashed line for **2α**; dotted line for **2β**. The thermally non-accessible paths of **1β** are not plotted. Lines are just a guide to the eye.

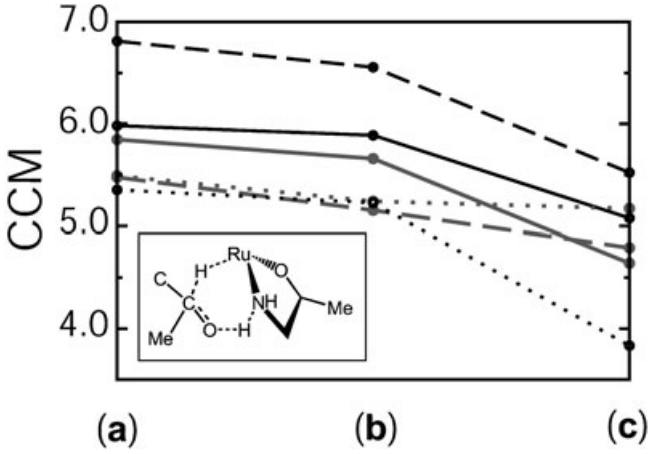


**Figure 6.** CCM of the relevant molecular subunit (inset shows schematic drawing) of the catalyst-substrate complex for the critical points along the reaction path of the acetophenone reduction. In black the path that gives the *S*-enantiomer; in red, the path that gives the *R*-enantiomer: solid line for **1α**; dashed line for **2α**; dotted line for **2β**. The plot for the thermally non-accessible paths of **1β** are not shown. Lines are just a guide to the eye.

state (which is ~2 kcal higher in energy). It may therefore be suggested that it is the nature of the intrinsic substrate that guides the reaction enantiomeric excess, and that the catalyst should adjust the conformation of the substrate in such a manner that it reaches the highest possible chirality.

## Conclusion

We have monitored the trends in chirality exchange/formation along ten reaction pathways of the ruthenium-catalyzed reduction of ketones by using density functional theory-optimized structures for chirality calculations, using Avnir's "continuous chirality measure". The catalyst's chirality measure does not *per se* differentiate between the enantiomeric pathways that give the major *S*- and the minor *R*-enantiomer. However, for acetophenone the catalysts are able to induce a gradient of chirality between the two paths that privileges the major enantiomer. These catalysts have two diastereomeric forms with the different chiralities at the ruthenium center, **α** (*R*) and **β** (*S*). The chirality measure analysis suggests that **α** gives *S*-1-phenylethanol and **β** produces *R*-1-phenylethanol. Comparison of the chirality measure values with the dihedral angles whose inversion changes the chirality agrees with the different behavior proposed for **α** and **β** catalysts. The better performance of catalyst **1** over catalyst **2** for the reduction of acetophenone is attributed to the fact that **2** exists in two diastereomeric forms that give preference to the opposite enantiomeric products. The lack of performance of catalyst **1** for the reduction of 2-hexanone is ascribed to its inability to generate a chirality difference/gradient in the substrate between paths that give mirror image enantiomers. Detailed analysis of the aromatic and aliphatic substrates shows that the conformation of the substrate in the transition state is of crucial importance. In the transition states, acetophenone is forced by the catalyst in a conformation with a higher chirality that facilitates enantio-in-

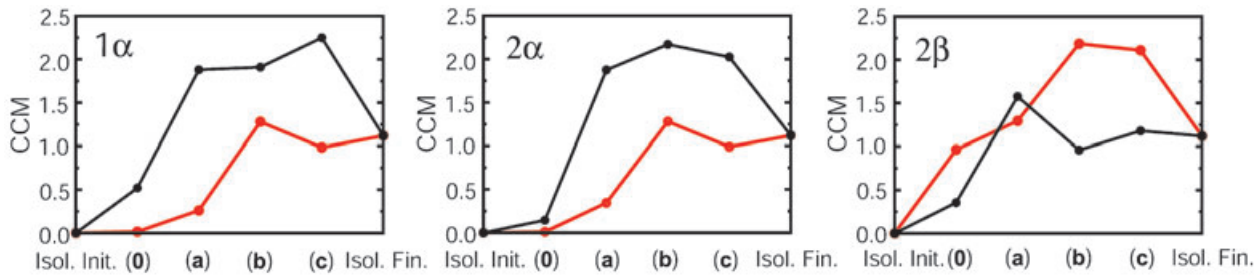


**Figure 5.** Substrate CCM along the reaction pathways of acetophenone reduction. In black the path that gives the *S*-enantiomer; in red, the path that gives the *R*-enantiomer. The plot for the thermally non-accessible paths of **1β** are not shown. Lines are just a guide to the eye.

  

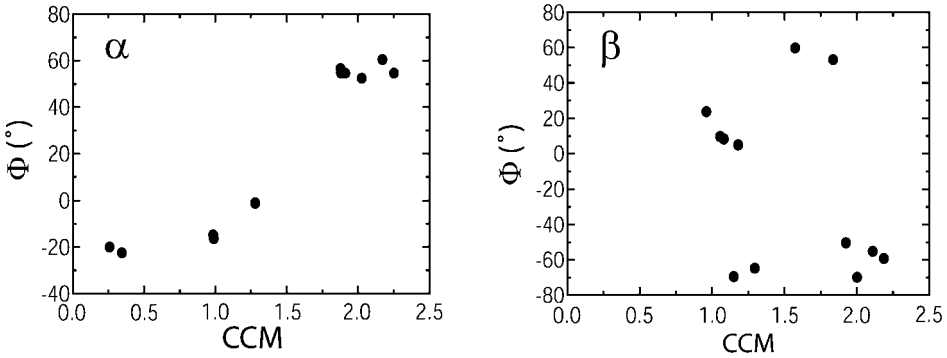


**Figure 7.** Substrate CCM for the reduction of acetophenone versus the $HC_{chiral}C_{phenyl}C_{phenyl}$ dihedral angle for the **α** (left) and **β** (right) catalysts. For simplicity, only the critical points (**a**), (**b**) and (**c**) are used.

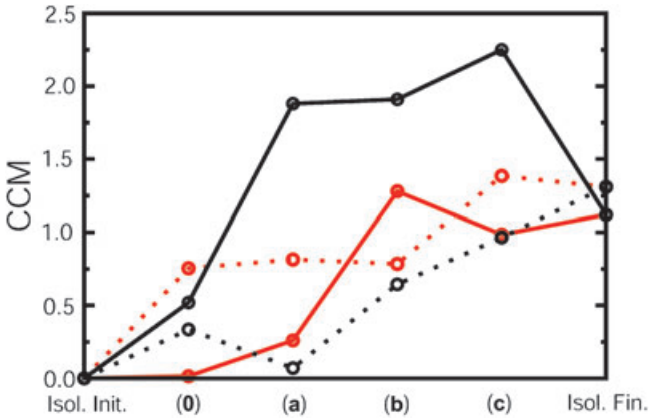


**Figure 8.** Acetophenone (solid line) and 2-hexanone (dotted line) CCM along the reaction pathway for **1α**. In black the path that gives the *S*-enantiomer; in red, the path that gives the *R*-enantiomer. Lines are just a guide to the eye.

duction. This type of information may be the key towards the rational design of catalyst for enantioselective conversion of inherently difficult substrates. We are currently exploring this idea and we are extending the approach to other enantioselective reactions.

## Acknowledgements

*J.-W. H. acknowledges NWO-CW (Nederlandse Organisatie voor Wetenschappelijk Onderzoek, Chemische Wetenschappen) through PIONIER. We acknowledge support from the Stichting Nationale Computerfaciliteiten (NCF) and the Nederlandse Organisatie voor Wetenschappelijk Onderzoek (NWO) for the use of supercomputer facilities.*

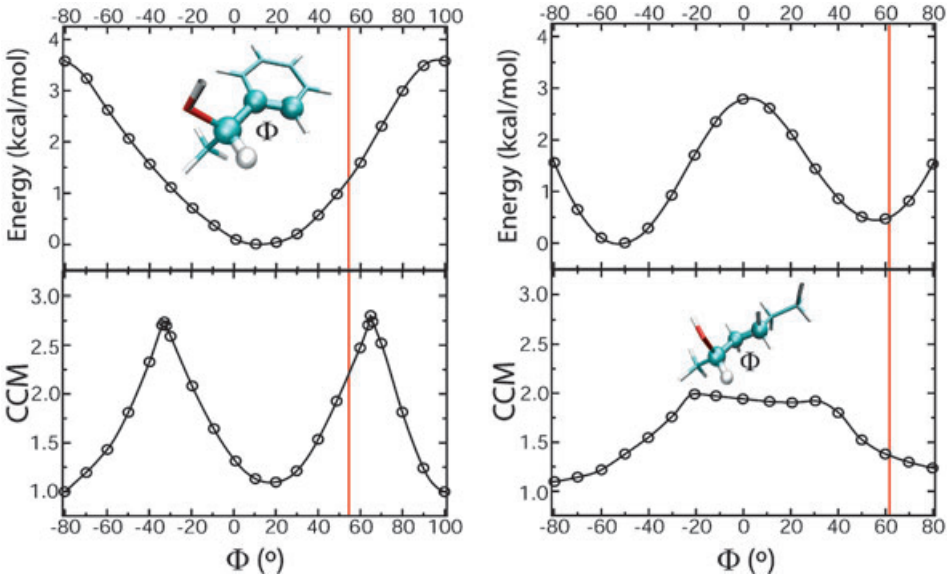


**Figure 9.** *Left:* Energy (*top*) and CCM (*bottom*) profiles for *S*-1-phenylethanol with a constrained dihedral angle Φ. The inset shows *S*-1-phenylethanol with the angle indicated in "ball and stick" mode; *Right:* Energy (*top*) and CCM (*bottom*) profiles for *S*-2-hexanol with a constrained dihedral angle Φ. The inset shows *S*-2-hexanol with the angle indicated in "ball and stick" mode. The red vertical lines indicate the actual dihedral angle of the substrates in the transition state of **1α**-*Re(S)*. Inversion of Φ gives the energy profile and change in CCM of the *R*-enantiomers.

  

## References


[1] P. E. Blöchl, A. Togni, *Organometallics* **1996**, *15*, 4125.

[2] a) D. Gleig, R. Schmid, W. A. Herrmann, *Organometallics* **1998**, *17*, 2141; b) D. Gleig, W. A. Herrmann, *Organometallics* **1999**, *18*, 4354; c) G. Ujaque, F. Maseras, A. Lledós, *J. Am. Chem. Soc.* **1999**, *121*, 1317; d) X. Wang, K. N. Houk, M. Spichty, T. Wirth, *J. Am. Chem. Soc.* **1999**, *121*, 8567; e) P.-O. Norrby, T. Rasmussen, J. Haller, T. Strassner, K. N. Houk, *J. Am. Chem. Soc.* **1999**, *121*, 10186.

[3] a) H. Zabrodsky, S. Peleg, D. Avnir; *J. Am. Chem. Soc.* **1992**, *114*, 7843; b) S. Keinan, D. Avnir, *J. Am. Chem. Soc.* **1998**, *120*, 6152.

[4] a) D. Gao, S. Schefzick, K. B. Lipkowitz, *J. Am. Chem. Soc.* **1999**, *121*, 9481; b) K. B. Lipkowitz, S. Schefzick, D. Avnir, *J. Am. Chem. Soc.* **2001**, *123*, 6710; c) K. B. Lipkowitz, C. A. D'Hue, T. Sakamoto, J. N. Stack, *J. Am. Chem. Soc.* **2002**, *124*, 14255.

[5] K. B. Lipkowitz, S. Schefzick, *Chirality* **2002**, *14*, 677.

[6] L. Bellarosa, F. Zerbetto, *J. Am. Chem. Soc*. **2003**, *125*, 1975.

[7] G. Zassinovich, G. Mestroni, S. Gladiali, *Chem. Rev.* **1992**, *92*, 1051.

[8] a) S. Hashiguchi, A. Fujii, J. Takehara, T. Ikariya, R. Noyori, *J. Am. Chem. Soc*. **1995**, *117*, 7562; b) R. Noyori, S. Hashiguchi, *Acc. Chem. Res.* **1997**, *30*, 97; c) K.-J. Haack, S. Hashiguchi, A. Fujii, T. Ikariya, R. Noyori, *Angew. Chem. Int. Ed. Engl.* **1997**, *36*, 285; d) S. Hashiguchi, A. Fujii, K.-J. Haack, K. Matsumura, T. Ikariya, R. Noyori, *Angew. Chem. Int. Ed. Engl.* **1997**, *36*, 288; e) K. Matsumura, S. Hashiguchi, T. Ikariya, R. Noyori, *J. Am. Chem. Soc*. **1997**, *119*, 8738; f) D. G. I. Petra, P. C. J. Kamer, A. L. Spek, H. E. Schoemaker, P. W. N. M. van Leeuwen, *J. Org. Chem*. **2000**, *65*, 3010; g) D. A. Alonso, S. J. M. Nordin, P. Roth, T. Tarnai, P. G. Andersson, M. Thommen, U. Pittelkow, *J. Org. Chem*. **2000**, *65*, 3116.

[9] a) D. A. Alonso, P. Brandt, S. J. M. Nordin, P. G. Andersson, *J. Am. Chem. Soc.* **1999**, *121*, 9580; b) M. Yamakawa, H. Ito, R. Noyori, *J. Am. Chem. Soc*. **2000**, *122*, 1466; c) D. G. I. Petra, J. N. H. Reek, J.-W. Handgraaf, E. J. Meijer, P. Dierkes, P. C. J. Kamer, J. Brussee, H. E. Schoemaker, P. W. N. M. van Leeuwen, *Chem. Eur. J.* **2000**, *6*, 2818; d) J.-W. Handgraaf, J. N. H. Reek, E. J. Meijer, *Organometallics* **2003**, *22*, 3150; e) M. Yamakawa, I. Yamada, R. Noyori, *Angew. Chem. Int. Ed. Engl.* **2001**, *40*, 2818.

[10] R. Noyori, M. Yamakawa, S. Hashiguchi, *J. Org. Chem.* **2001**, *66*, 7931.

[11] A. D. Becke, *Phys. Rev. A* **1988**, *38*, 3098.

[12] C. Lee, W. Yang, R. G. Parr, *Phys. Rev. B* **1988**, *37*, 785.

[13] N. Troullier, J. L. Martins, *Phys. Rev. B* **1991**, *43*, 1993.

[14] CPMD, version 3.4, developed by J. Hutter, A. Alavi, T. Deutsch, M. Bernasconi, St. Goedecker, D. Marx, M. Tuckerman, M. Parrinello, MPI für Festkörperforschung and IBM Zurich Research Laboratory, **1995–1999**.

[15] ADF 2000, G. te Velde, E. J. Baerends et al., Theoretical Chemistry, Vrije Universiteit, Amsterdam.

[16] a) G. Brancato, F. Zerbetto, *J. Phys. Chem. A* **2000**, *104*, 11439; b) M. Asakawa, G. Brancato, M. Fanti, D. A. Leigh, T. Shimizu, A. M. Z. Slawin, J. K. Y. Wong, F. Zerbetto, S. Zhang, *J. Am. Chem. Soc.* **2002**, *124*, 2939; c) G. Brancato, F. Coutrot, D. A. Leigh, A. Murphy, J. K. Y. Wong, F. Zerbetto, *Proc. Natl. Acad. Sci. USA* **2002**, *99*, 4967.

[17] S. Alvarez, S. Schefzick, K. B. Lipkowitz, D. Avnir, *Chem. Eur. J.* **2003**, *9*, 5832.

[18] D. G. I. Petra, *Asymmetric Transfer Hydrogenation of Ketones*, Thesis, University of Amsterdam, Institute of Molecular Chemistry, 1999.


  